Nanoscale

Accepted Manuscript

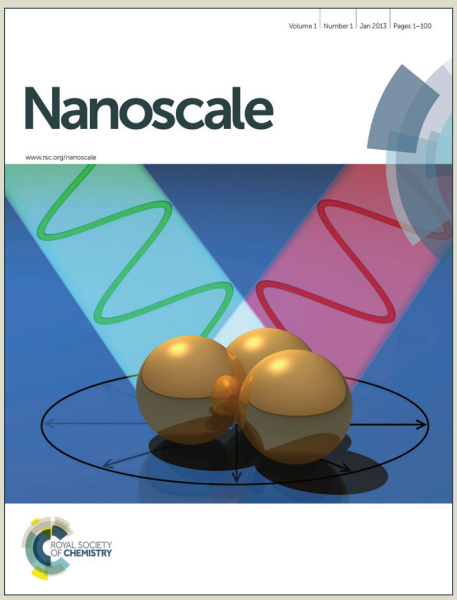

ROYAL SOCIETY OF CHEMISTRY

www.rsc.org/nanoscale

Highly sensitive pressure sensor using a double-layer graphene structure for tactile sensing

Sungwoo Chun, Youngjun Kim, Hyeong-Sik Oh, Giyeol Bae and Wanjun Park*

Department of Electronic Engineering, Hanyang University, Seoul 133-791, South Korea

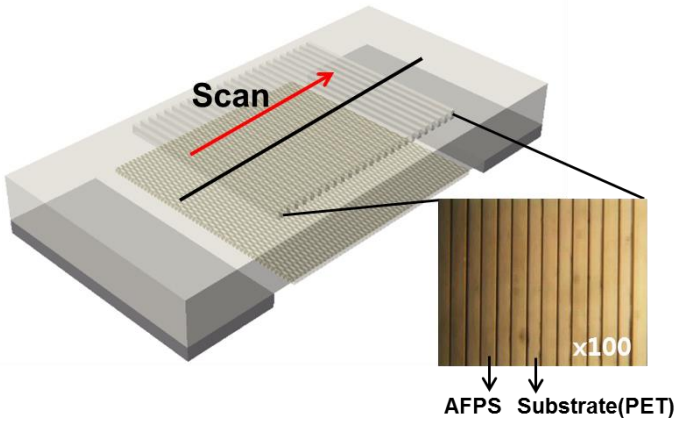

The sensor adopting the electromechanical characters of single-layer graphene recognizes surface morphology. Tactile sensing for the sensor is demonstrated in the frequency scale of human perception induced by gentle touching.

Abstract

In this paper, we propose a graphene sensor using two separated single-layer graphenes on a flexible substrate for use as a pressure sensor, such as for soft electronics. The working pressure corresponds to the range in which human perception recognizes surface morphologies. A specific design of the sensor structure drives the piezoresistive character due to the contact resistance between two graphene layers and the electromechanical property of graphene itself. Accordingly, sensitivity in resistance change is given by two modes for low pressure (-0.24/kPa) and high pressure (0.039/kPa) with a crossover pressure (700 Pa). This sensor can detect infinitesimal pressure as low as 0.3 Pa with uniformly applied vertical force. With attachment of the artificial fingerprint structure (AFPS) on the sensor, the detection ability for both the locally generated shear force and actual human touch confirms recognition of the surface morphology constructed by periodic structures.

***Correspondence to:** wanjun@hanyang.ac.kr

Introduction

With their use of flexible, stretchable, and transparent substrate on which electrical components are integrated, soft electronics are expected to expand their application area to wide varieties of human-friendly electronic systems, such as wearable electronics [1-3], electronic skin [4-9], foldable touch screens [10-11], and flexible surgical robots [12]. The highly sensitive pressure sensor is a fundamental electronic element in this area for both the input and detection by devices of human-generated signals [13-14]. Tactile sensing, in particular, which enables the perception of surface topologies and hardness, is essential to achieving the electrical recognition of the touch sensation. For example, electronic skin imitates the perceptual processes of human touch by mechanoreceptors in the skin over a wide pressure range (100 Pa–10 kPa) [15-16]. Moreover, a highly sensitive working capability below 100 Pa should be an advantage for recognizing tactile information beyond the human sense range. To attain such a highly sensitive sensor on the flexible substrate, piezoelectric polymers [17], grid-structured nanowires [2, 18], and graphenes [19-23] have been studied to take advantage of their sensitive electromechanical character and structural flexibility.

Among the candidate materials, graphene could be most suitable for the architecture of soft electronics because fabrication of the sensor element and array is not limited to using the standard process of micro-devices. Moreover, the strong mechanical property known as 1 TPa for the mechanical strength, and 130 GPa of the intrinsic breaking strength [24-25], enables the adoption of single-layer graphene (SLG) for the device element operated by mechanical input. The effect of strain on the resistance of SLG represents the electromechanical behavior due to distortion of the crystal structure, which results in modification of the electronic structure and mobility reduction [26-29]. The gauge factor (GF), defined as the ratio of resistance change per elastic strain, has been measured up to 6.1 [27, 30-31]; however, for the

actual pressure sensor, it should be treated by vertical pressure with its advantages. An *in situ* nanoindentation experiment showed that strain driven by a vertical force yielded a GF of ~1.9 for free-standing SLG without a supporting substrate [32]. Although such a low GF is a disadvantage for the pressure sensor that employs SLG, it can be overcome by the introduction of a pressure-amplifying structure in the sensor design [21].

We propose a graphene pressure sensor for tactile sensing using two separated SLGs (double-layer graphene [DLG]) on a flexible substrate with a working pressure that covers the human perception range; the lowest working pressure is as low as 0.3 Pa. The sensor has two distinguishable operating mechanisms for working pressure: 1) contact-area dominance between each SLG for the low pressure regime (< ~250 Pa), which gives a pressure sensitivity of -0.24/kPa; and 2) electromechanical property dominance for the high pressure regime (> ~1000 Pa), which gives 0.039/kPa. With confirmation of sheer force detection, tactile sensing is evaluated in frequency responses after attachment of an artificial fingerprint structure (AFPS) on the sensor. The proposed sensor provides a unique feature to recognize the surface morphology of the contacting materials in difference with the previously studied force sensors for the flexible scheme.

Results and discussion

Fig. 1a illustrates the process of preparing the sensor. SLG is obtained from a direct growing method by thermal chemical vapor deposition (CVD) and is transferred to a polydimethylsiloxane (PDMS) substrate by a polymethyl-methacrylate (PMMA) assisted dry transfer method [22]. After setting up a PDMS pillar, Pt electrodes are introduced. The second SLG on the PMMA substrate is assembled to make a DLG structure isolated by the PDMS pillar. The fabrication details are described in Supporting Information: S1. **Fig. 1b** displays the completed sensor. Since the second SLG on the PMMA is attached on the first

SLG through the standard wet process, the contact area between two SLGs is naturally formed by bending due to the weight of PMMA during this process. The contact area is estimated as ~ 6 x 6 mm in length (X) and width for the height of the PDMS stand of 1.4 mm. Then, the contact force between two SLGs is strong enough to keep this contacting structure when the sensor is turned upside down. The PDMS substrate practically acts as the absorber of forces for detection. The bottom SLG on the PMMA freely stands with the support of the pillar. The height of the stand determines the contact area with the top SLG, which is strongly combined with the PDMS substrate through the PMMA interlayer. Before pressing, the resistance (R_0) of the sensor is defined by the natural contact between the SLGs. Applied force induces both a contact area increase (ΔX) and distortion of the graphene atomic structure by stretching (ΔY). These results in the piezoresistive effect ($R = R_0 + \Delta R$) of the sensor in two ways: positively for the contact effect, and negatively for the electromechanical effect, of graphene.

Fig. 2 shows the piezoresistive response for the vertical pressure input of 11.8 to 10,000 Pa, which can be generally generated by the internal human organics or perceived by human tactile mechanoreceptors. For measurement accuracy, a weight staking method is employed with a PDMS weight (75.5 mg) with a dimension of 8x8 mm^2, which uniformly applies 11.8 Pa to the sensor with a single stack. The measurement is performed with the weight at the center of the sensor where the contact areas between graphene and electrode are isolated for the direct applied force. In the low pressure regime (< ~700 Pa), reduction of electrical resistance with increasing vertical pressure contributes to the decrease of contact resistance due to the contact area increase between the top and bottom SLGs [22]. The rate ($(\Delta R/R_0)/\Delta P$) that describes sensitivity of the piezoresistive response for the pressure sensor is estimated as -0.24 kPa^{-1} from the rough linear tendency below ~250 Pa. However, the resistance increases with the increase of vertical pressure above the applied pressure (> ~700 Pa). The distortion

of C-C bonds due to vertical strain in the bottom SLG results in a higher resistance increase than reduction of resistance by the additional contact area. The pressure sensitivity is estimated as 0.034 kPa^{-1} for the linear response range of 1 to 8 kPa. The sensor adopting two operational modes is attributed to the positive and negative sensitivities. It inevitably result a crossover pressure that indicates the turning point of the negative sensitivity to the positive. The crossover pressure accompanies a pressure region where sensor output is not clearly distinguished because output of the sensor could be measured with a same value for different applied pressures. The range of 250 ~ 600 Pa with ~ 300 Pa of the crossover pressure is observed from the presented sensor. It is noted that achievement of high (positive) sensitivity after the crossover pressure is required to reduce this ambiguous pressure region.

Because the substrate (PDMS) is also a flexible material, the applied vertical pressure induces its structural deformation, which additionally affects the piezoresistive response for the sensor. Such effects for the two modes are simply tested with the thickness of the substrate (see Supporting Information: S2 for details). Observation indicates that the sensor becomes less sensitive for both working modes as the thickness is increased because the input force is absorbed in the substrate rather than transferred to the graphene layers.

The sensor that uses the 600-μm thick PDMS substrate can, in fact, detect infinitesimal pressure as low as 0.3 Pa driven by a paper sheet with a weight of 5.25 mg, as described in **Fig. 3**a. The resistance change by the piezoresistive response ($\Delta R/R_0$) is read as -0.001. It is noted that this sensor ability is unique for such low pressure detection compared to pressure sensors previously reported for the flexible scheme [5, 15, 20, 33-34].

Fig. 3b shows the resistance change for the response in time to the application of pulsed pressure (118 Pa driven by the weight corresponding to 10 PDMS stacks) with both on and off durations of 1.5 s and consecutive measurements at every 40 ms interval. The initial resistance (R_0) of the sensor is measured as 17.0 kΩ. The resistance decreases to 16.2 kΩ

after applying the vertical force, resulting in a resistance change ($\Delta R/R_0$) of ~ -0.05. After the applied force is removed, the sensor instantly recovers to its initial value within a few tenths of a millisecond, followed by the relaxing action of the PDMS substrate.

As an example, monitoring the pulse beat is tested for the method to confirm the detection ability of the human-generated signal with the sensor. To detect the wrist pulse, it is attached on the wrist and positioned on the radial artery. **Fig. 3**c shows a pulse train with a rate of 65 min^{-1}. The shape of the single pulse isolated from the pulse train in **Fig. 3**d describes additional information. First of all, the single pulse represents a full waveform featured by the two main components of the wave generated by the heart. These are attributed to the forward moving wave (ejected wave) and the reflected wave when it contracts, and it respectively travels along the arterial walls. The maximum amplitudes, known as the systolic top and the diastolic top, are also featured in the sensor output. The measured practical value for ~4% of the resistance decrease indicates that pressure due to the systolic top on the wrist is approximately 100 Pa. The pressure rate (P_2/P_1) of the diastolic top to the systolic top, which is denoted as the radial augmentation index that indicates the heart health status [35], can be estimated as 0.54 from the sensor output.

Tactile sensing basically requires generation of the output signal, including information for the surface morphologies. The sensor should work for the shear force induced by the slip motion of the tested material with surface roughness. **Fig. 4**a depicts a schematic of measuring the local shear force with the sensor with a flexible PET bump (width = 100, height = 50 μm) that is introduced on the PDMS substrate. The vertical force through the PET tip (width = 120 μm) generates a local shear strain on the sensor when the PET tip touches the bumper during the slip motion. **Fig. 4**b shows the piezoresistive responses for the applied force with different scan velocities (0.1–2 mm/min). Slow slip motion (0.1 mm/s) for the single bumper accurately estimates the tip width as 0.13 mm from evaluation of moving

distance during the contacting with 1.3 sec of the pulse width. However the cases for v = 0.5, 1, 2 mm/sec give the estimated widths of 0.3, 0.2, 0.2 mm which are larger than actual width of the tip. It implies that time delay is inevitably contained in the sensor response for the slip motion, which is attributed to the microscopic origins such as friction between surfaces of the PET tip and bumper, and the viscoelastic effect of PET. Especially, the bending for both of the PET tip and bump due to the viscoelastic effect makes a disturbance for sharp termination of the response pulses. For the double bump case, the time for completion of touching is equivalent to the time for moving the distance (width of two bumps + width of tip = 0.420 mm) of the tip. It should be 4.2, 0.8, 0.4, 0.2 sec for the moving speed of 0.1, 0.5, 1, 2 mm/s, respectively. But measurement results 4.0, 2.0, 1.2, 0.6 sec for the same order of the moving speeds. The increase of resistance with the shear force indicates that the sensor is operating in the high pressure regime. Thirty percent of resistance change is equivalent to the value induced by 1.7 kPa of vertical pressure directly applied to the sensor. However, this force in a real situation is very locally applied on the graphene layer beneath the PET bump in contrast to the case of the uniformly applied vertical pressure measurement. The performance details of the sensor in the high pressure regime are presented in Supporting Information: S3. The geometrical features of the bump are represented by the scanning velocity for the slip motion; two bumps (pitch = 100 μm) in the sensor are recognized through the piezoresistive output signals due to the shear strain.

The transfer of shear force to the sensor is an important factor for detecting surface morphologies. To establish the texture characteristics of the tested materials, we introduce periodic ridges on the sensor, which serve as an AFPS. The PET is chosen for the AFPS because its Young's modulus (~ 4 GPa) is higher than that of the PDMS (~ 2 MPa). The AFPS patterns are formed by conventional photolithography using SU-8 for the photoresist and reactive ion etching (RIE) with CF_4. **Fig. 5**a shows a schematic of the completed sensor

with the AFPS whose size is 100 and 50 μm for line width and height, respectively; the distance between ridges is 200 μm. Touching event on the AFPS by the PET tip generates the in-plane force to the sensor that is transferred to the graphene layers through structural deformation of the PDMS. **Fig. 5**b depicts responses for the scanning motion of the PET tip on the sensor in the frequency domain of 5–50 Hz, which corresponds to the human perception range. The periodic structure of the AFPS contributes to the observed peak positions in the wave patterns of the fast Fourier transform (FFT) with the resistance response of the sensor. The peak frequencies (f) resulting from the different slip speeds (v) of 4, 6, and 8 mm/s are 22, 30, and 41 Hz, respectively, which accurately represent the periodic distance (v / f = 200 μm) of the AFPS.

At this point, the sensor is tested for surface morphology recognition. Scanning is simply performed by gentle rubbing of the test structures attached to the human finger. **Fig. 6**a shows the FFT wave pattern generated by regular copy paper as a reference for the smooth surface with a non-periodic surface texture. As expected, no specific peak appears in the FFT wave pattern. **Fig. 6**b and **6**c show cases for the test samples whose surface textures are periodic. For the test sample constructed with the identical periodic structure of the AFPS, peaks are concentrated at the single frequency referring to ~30 Hz, which corresponds to 6 mm/s for the rubbing speed. The apparent multiple peaks are attributed to slight differences due to process variations in distances between patterns for both the test sample and AFPS in the sensor. The test surface with 400 μm of the periodic distance (line width = 200 μm, pitch = 200 μm) shows two meaningful peaks at 14 Hz and 28 Hz in the FFT wave pattern. Because the peak appearing at 28 Hz is apparently due to the AFPS, 400 μm of the periodic distance for the test surface should result in a peak at 14 Hz. The direct sensor responses in current for the test samples are presented in Supporting Information: S4. **Fig. 6**d shows the sensor response for a

human fingertip. The structure of this also produces a periodic surface; however, it is not perfect. Distances between the patterns are specified in the range of 400–800 μm; moreover, curvatures for the pattern deviate from the perfect periodic structure above the test surfaces. Therefore, it could be a good test surface for the sensor. The peak from the AFPS is read at 23 Hz with a scan speed of 4.6 mm/s. The deviations from the periodic structure result in several peaks distributed at 4–12 Hz.

Conclusions

In summary, we have proposed a sensor for detecting the pressure range of human perception as low as 0.3 Pa with a specific structure of two single-layer graphenes. The sensor features two distinct operating mechanisms across the crossover pressure range. The sensitivity shows -0.24 kPa^{-1} below 250 Pa and 0.039 kPa^{-1} above 700 Pa with uniformly applied vertical pressure on the whole area of the sensor. This sensor is extendable for detecting human-generated signals as a force-sensing element in wearable electronics. Furthermore, the response characteristics for shear force locally applied on the sensor generate distinguishable signals with the slip motion. This observation enables introduction of the artificial fingerprint structure on the sensor. Recognition of the surface morphology can then be demonstrated for tactile sensing in the frequency scale of human perception induced by gentle touching.

Experimental

1. Sensor fabrication

Single-layer graphene was obtained from a direct growing method by thermal chemical vapor deposition (CVD) on a catalytic metal of 25-um-thick copper foil (purity: 99.8%, Alfa Aesar Co.). A 150-nm-thick polymethyl-methacrylate (PMMA, 950K, C4, Micro Chem. Co.) on the as-grown graphene layer was introduced to enhance the adhesion strength between the graphene layer and a PDMS substrate because the adhesion energy of graphene on PMMA (66 mJ/m^2) is greater than that of graphene on PDMS (41 mJ/m^2) [36]. Conventional copper etching by $FeCl_3$ solution was conducted for 1 h. Cleaning to remove copper residues was accompanied with the cleaning processes using the standard clean (SC)-1 and the standard clean (SC)-2 [37]. After raising 1-cm thickness of the PDMS stand on both sides, an 80-nm-thick Pt layer was deposited on the PDMS stand by the sputtering method with a stencil mask for electrode formation. The transfer of the graphene layer onto the PDMS substrate was confirmed through Raman resonance, which indicated typical single-layer graphene with a reasonably small ratio of intensities (~0.33) of the G band (1587 cm^{-1}) to the 2D band (2682 cm^{-1}). Wet transfer was introduced to cause the double-layer graphene to have free-standing graphene on both sides of the PDMS stand. Finally, PMMA residues on wet-transferred graphene were removed by acetone for 10 min. Both contacts were again deposited by the sputtering method to improve their contact properties. The transmittance measurement showed ~91.7% at 550 nm with ~5% transmittance loss by the double-layer graphene.

2. Fabrication of artificial fingerprint structure (AFPS) and periodic structures on the test sample surfaces

125-μm-thick terephthalate (PET) was chosen as the substrate material for both the AFPS and test samples. A spin coating method (3,000 rpm) was used for the SU-8 photoresist on the PET substrate; two step curing processes (65℃, 3 min and 95℃, 9 min) followed.

Conventional optical lithography was conducted for the photoresist strip of 75 μm in height. Preparation of the samples was completed with a reactive ion etching process, which was accompanied by 30 sccm of CH_4 gas and 150 W of plasma power. The resulting height for both the AFPS and periodic structures on the test sample surfaces was 50 μm.

3. Method of measurement

Detection of tactile signals in time was conducted by X-axis Autostage for scanning the longitudinal (lateral) direction in the velocity range of 1–5000 mm/min by the homemade apparatus (see Supporting Information: S5 for details). The Keithley 2400 sourcemeter communicating with the measurement apparatus is used for measurement of electrical recordings with two contact channels of the sensor devices. Finally, the piezoresistive oscillation of the resistance by scanning the sensor surface was converted a form of the frequency domain by fast Fourier transform (FFT) in the Matlab software.

Supporting information

Supporting information is available.

Acknowledgements

This work was supported by the NRF of Korea (2012M3A7B4035195, 2009-0083540).

References and notes

1. C. Pang, C. Lee, K.-Y. Suh, *J. Appl. Polym. Sci.* 2013, 130, 1429.
2. S. Gong, W. Schwalb, Y. Wang, Y. Chen, Y. Tang, J. Si, B. Shirinzadeh, W. Cheng, *Nat. Commun*. 2013, 5, 3132.
3. M. J. Cima, *Nat. Biotechnol*. 2014, 32, 642.
4. M. L. Hammock, A. Chortos, B. C.-K. Tee, J. B.- H. Tok, Z. Bao, *Adv. Mater*. 2013, 25, 5997.
5. X. Wang, Y. Gu, Z. Xiong, Z. Cui, T. Zhang, *Adv. Mater*. 2014, 26, 1336.
6. A. N. Sokolov, B. C.-K. Tee, C. J. Bettinger, J. B.-H. Tok, Z. Bao, *Acc. Chem. Res.* 2012, 45, 361.
7. J. J. Boland, *Nat. Mater*. 2010, 9, 790-792.
8. M. Ramuz, B. C.-K. Tee, J. B.-H. Tok, Z. Bao, *Adv. Mater*. 2014, 24, 3223.
9. S. Bauer, S. Bauer-Gogonea, I. Graz, M. Kaltenbrunner, C. Keplinger, R. Schwodiauer, *Adv. Mater*. 2014, 26, 149.
10. H.-J. Kwon, H. Shim, S. Kim, W. Choi, Y. Chun, I. Kee, S. Lee, *Appl. Phys. Lett*. 2011, 98, 151904.
11. S. Kim, H.-J. Kwon, S. Lee, H. Shim, Y. Chun, W. Choi, J. Kwack, D. Han, M. Song, S. Kim, S. Mohammadi, I. Kee, S. Y. Lee, *Adv. Mater*. 2011, 23, 3511.
12. S. Horgan, K. Thompson, M. Talamini, A. Ferreres, G. Jacobsen, G. Spaum, J. Cullen, L. Swanstrom, *Surg. Endosc*. 2011, 25, 586.
13. D.-H. Kim, N. Lu, R. Ma, Y.-S. Kim, R.-H. Kim, S. Wang, J. Wu, S. M. Won, H. Tao, A. Islam, K. J. Yu, T.-I. Kim, M. Chowdhury, M. Ying, L. Xu, M. Li, H.-J. Chung, H. Keum, M. McCormick, P. Liu, Y.-W. Zhang, F. G. Omenetto, Y. Huang, T. Coleman, T. A. Rogers, *Science* 2011, 333, 838.
14. R. S. Dahiya, G. Metta, M. Valle, G. Sandini, *IEEE Trans. Robot*. 2010, 26, 1.
15. S. C. Mannsfeld, B. C.-K. Tee, R. M. Stoltenberg, C. V. H.-H. Chen, S. Barman, B.V. O. Muir, A. N. Sokolov, C. Reese, Z. Bao, *Nat. Mater*. 2010, 9, 859.
16. E. S. Dellon, R. Mourey, A. L. Dellon, *J. Plast. Reconstr. Surg*. 1992, 90, 112.
17. K. S. Ramadan, D. Sameoto, S. Evoy, *Smart Mater. Struct*. 2014, 23, 03301.
18. K. Takei, T. Takahashi, J. C. Ho, H. Ko, A. G. Gillies, P. W. Leu, R. S. Fearing, A. Javey, *Nat. Mater.* 2010, 9, 821.
19. H.-B. Yao, J. Ge, C.-F. Wang, X. Wang, W. Hu, Z.-J. Zheng, Y. Ni, S.- H. Yu, *Adv. Mater*. 2013, 25, 6692.
20. B. Zhu, Z. Niu, H. Wang, W. R. Leow, H. Wan, Y. Li, L. Zheng, J. Wei, F. Huo, X. Chen., *Small* 2014, 10, 3625.
21. S. Chun, Y. Kim, H. Jin, E. Choi, S.-B. Lee, W. Park, *Carbon* 2014, 78, 601.
22. S. Chun, Y. Kim, H. Jung, W. Park, *Appl. Phys. Lett.* 2014, 105, 041907.
23. S.-E. Zhu, M. K. Ghatkesar, C. Zang, G. C. A. M. Janssen, *Appl. Phys. Lett*. 2013, 102, 161904.
24. C. Lee, X. Wei, J. W. Kysar, J. Hone, *Science* 2008, 321, 385.
25. K. S. Kim, Y. Zhao, H. Jang, S. Y. Lee, J. M. Kim, K. S. Kim, J.-H. Ahn, P. Kim, J.-Y. Choi, B. H. Hong, *Nature* 2009, 457, 706.
26. V. M. Pereira, A. H. C. Neto, *Phys. Rev. B* 2009, 80, 045401.
27. D. Yoon, Y.-W. Son, H. Cheong, *Phys. Rev. Lett*. 2011, 106, 155502.
28. X.-W. Fu, Z.-M. Liao, J.-X. Zhou, Y.-B. Zhou, H.-C. Wu, R. Zhang, G. Jing, J. Xu, X. Wu, W. Guo, D. Yu, *Appl. Phys. Lett*. 2011, 99, 213107.
29. T. Yu, Z. Ni. C. Du, Y. You, Y. Wang, Z. Shen, *J. Phys. Chem. C* 2008, 112 12602.
30. Y. Lee, S. Bae, H. Jang, S. Jang, S.-E. Zhu, S. H. Sim, Y. I. Song, B. H. Hong, J.-H. Ahn,

Nano Lett. 2010, 10, 490.
31. Y. Wang, R. Yang, Z. Shi, L. Zhang, D. Shi, E. Wang, G. Zhang, *ACS nano* 2011, 5, 3646.
32. M. Huang, T. A. Pascal, H. Kim, W. A. Goddard. Ⅲ, J. R. Greer, *Nano Lett*. 2011, 11, 1241.
33. L. Pan, A. Chortos, G. Yu, Y. Wang, S. Isaacson, R. Allen, Y. Shi, R. Dauskardt, Z. Bao, *Nat. Commun*. 2013, 5, 3002.
34. C.-L. Choong, M.-B. Shim, B.-S. Lee, S. Jeon, D.-S. Ko, T.-H. Kang, J. Bae, S. H. Lee, K.-E. Byun, J. Im, Y. Jeong, C. E. Park, J.-J. Park., U.-I. Chung, *Adv. Mater*. 2014, 26, 3451.
35. W. W. Nichols, *Am. J. Hypertens*. 2005, 18, 3S.
36. J. Song, D.-Y. Kam, R.-Q. Png, W.-L. Seah, J.-M. Zhuo, G.-K. Lim, P. K. H. Ho, L.-L. Chua, *Nat. Nanotechnol*. 2013, 8, 356.
37. X. Liang, B. A. Sperling, I. Calizo, G. Cheng, C. A. Hacker, Q. Zhang, Y. Obeng, K. Yan, H. Peng, Q. Li, X. Zhu, X. X. U. Yuan, H. Yuan, A. R. Hight Walker, Z. Liu, L.-M. Peng, C. A. Richter, *ACS nano* 2011, 5, 9144.

Figure caption

Fig. 1. (a) Summary of the process for the graphene pressure sensor: (1) single-layer graphene growth and attachment of PDMS onto a PMMA-coated graphene layer, (2) removal of catalytic Cu foil, (3) SC-2 treatment after removal of Cu residues by SC-1, (4) attachment of the PDMS pillar on both sides of the device, (5) formation of contact electrodes (Pt) on the PDMS pillar by a sputtering system, (6) bottom graphene wet transfer, and (7) removal of PMMA and re-deposition of Pt contact. (b) Photography of completed pressure sensor (left) and schematic representing the operating mechanisms in applied vertical pressure (right). The sensors feature two ways of contributing sensitivity: positively for the contacting effect (X) and negatively for the electromechanical effect of graphene (Y).

Fig. 2. Three cycle piezoresistive responses of the graphene pressure sensor under vertical pressure input of 11.8 to 10,000 Pa. In the low pressure regime (< 600 Pa), the sensor shows reduction of electrical resistance with increasing vertical pressure due to an increase of contact area between the top and bottom graphenes. However, the resistance increases with an increase of vertical pressure above the applied pressure (> ~700 Pa) by elongation of C-C bonds in the stretches in the bottom SLG.

Fig. 3. (a) Transient response to the application of a copy paper of 5.25 mg weight loaded on the surface of the sensor from 1.7 cm^2 (corresponding to 0.3 Pa), resulting in a resistance change by the piezoresistive responses of ~0.001. (b) Piezoresistive response in the low pressure regime. 10 PDMS stacks corresponding to 118 Pa is used for the application of pulsed pressure with both on and off durations of ~1.5 s; it exhibits a highly distinct response in the resistance change ($\Delta R/R_0$: ~ -0.05). (c and d) Monitoring of the wrist pulse. A pulse rate of 65 min^{-1} was obtained with an average resistance change of ~4%, corresponding to pulsed pressure of 100 Pa. The pressure rate (P_2/P_1) of the diastolic top to the systolic top denoted as the radial augmentation index, which indicates the heart health status, can be estimated as 0.54.

Fig. 4. (a) Schematic for measuring shear force with the sensor for rubbing a single flexible PET bumper attached on the sensor. For illustration purposes, the scale of the PET bumper and PET tip is magnified hundred times for comparing the distance between the electrodes. (b) Piezoresistive responses with different scan velocities (0.1–2 mm/min) for the single PET bumper and two PET bumpers. (Inset) SEM image of single PET bumper.

Fig. 5. (a) Schematic of completed sensor with the AFPS whose size is 100 and 50 μm for line width and height, respectively; the distance between ridges is 200 μm. (b) Responses for the scanning motion of the PET tip in the frequency domain of 5–50 Hz. The circles indicate peaks from the periodic feature of the testing surface.

Fig. 6. FFT wave patterns generated by (a) a regular copy paper as a reference with non-periodic surface texture, (b and c) test samples whose surface textures are periodic (200 μm and 400 μm respectively), and (d) a human fingertip. Each peak represents the surface characteristics upon gentle touching with the sensor. The circle in (b) indicate peaks from the periodic features of the testing surface and the AFPS. The first and second circles in (c) indicate peaks from the periodic features of the testing surface and the AFPS, respectively. The arrowed line and circle in (d) indicate peaks from the human finger print and the AFPS, respectively.

Figures

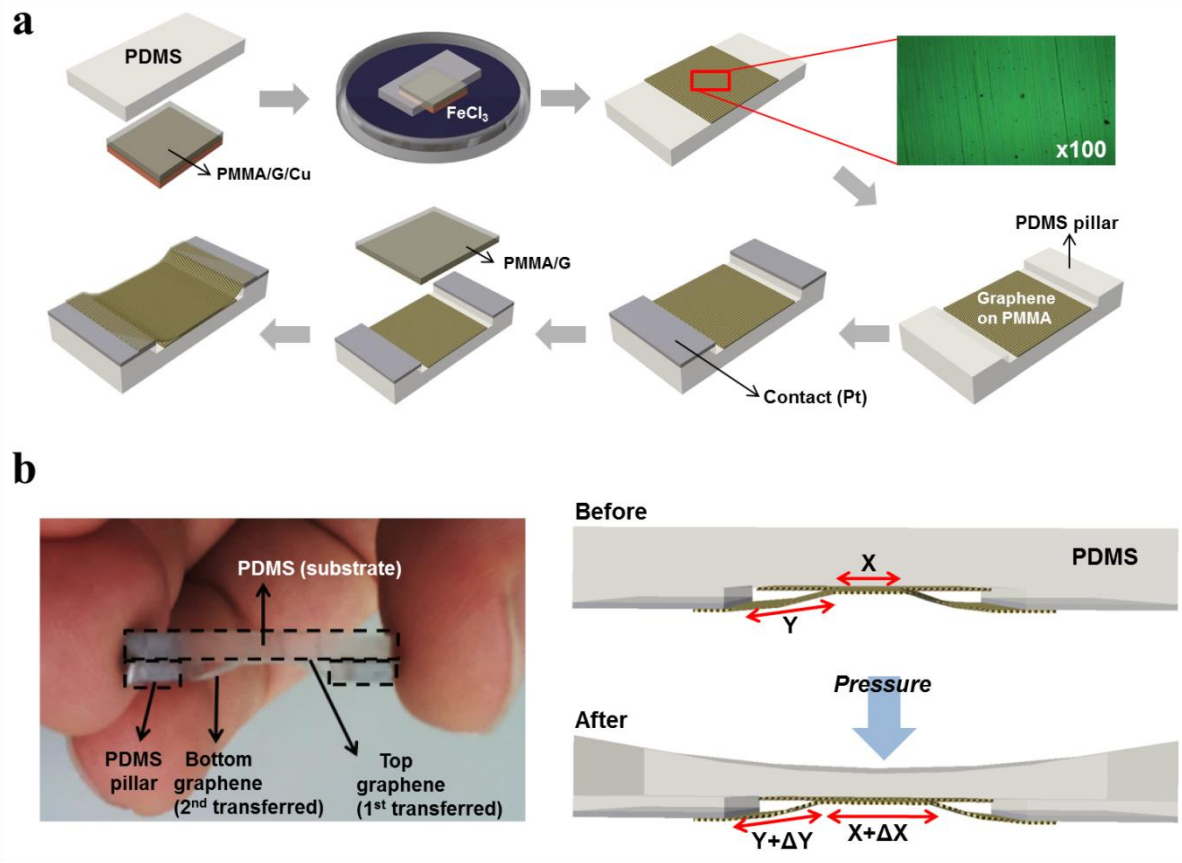

Fig. 1

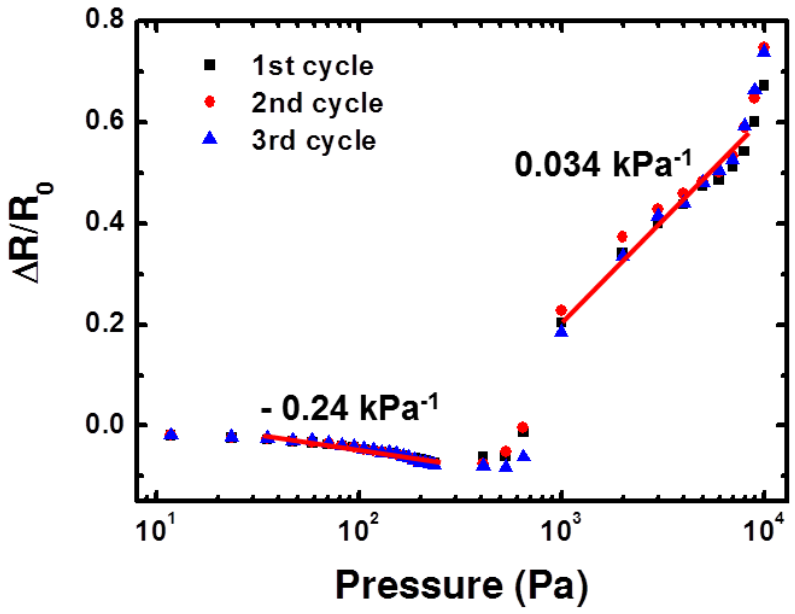

Fig. 2

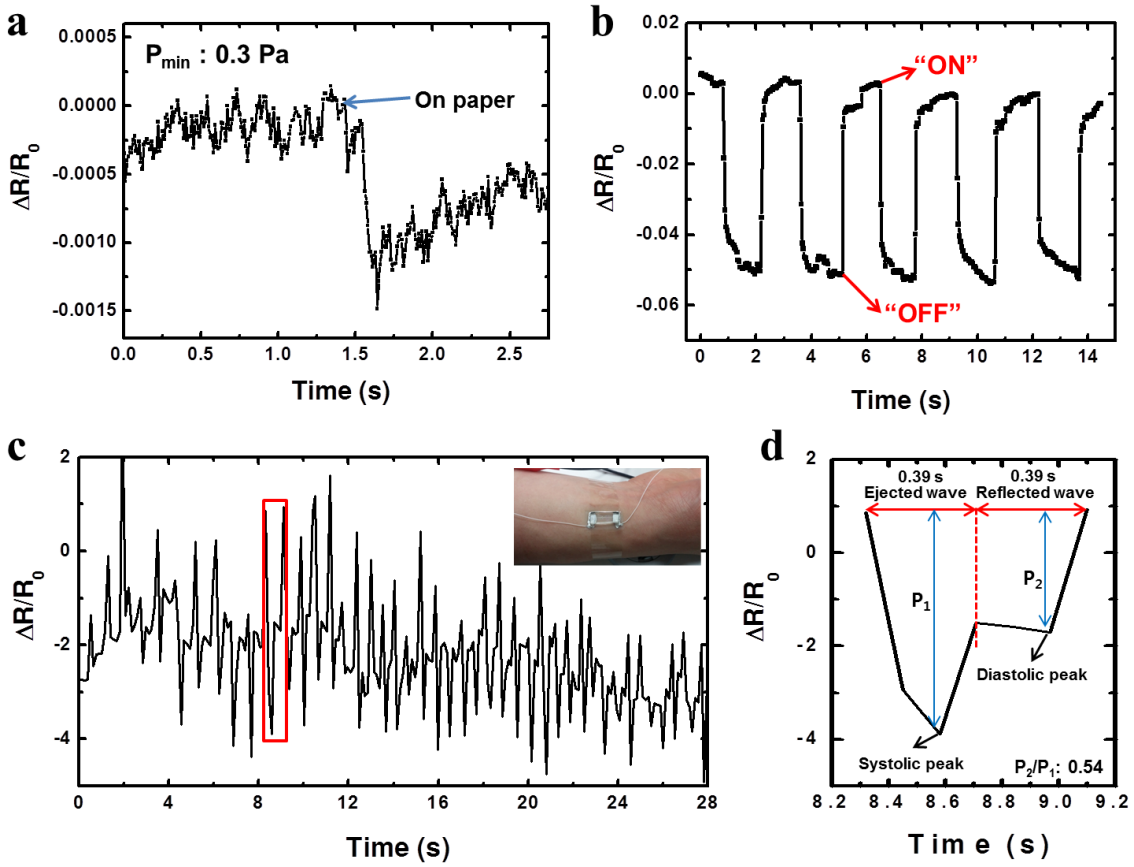

Fig. 3

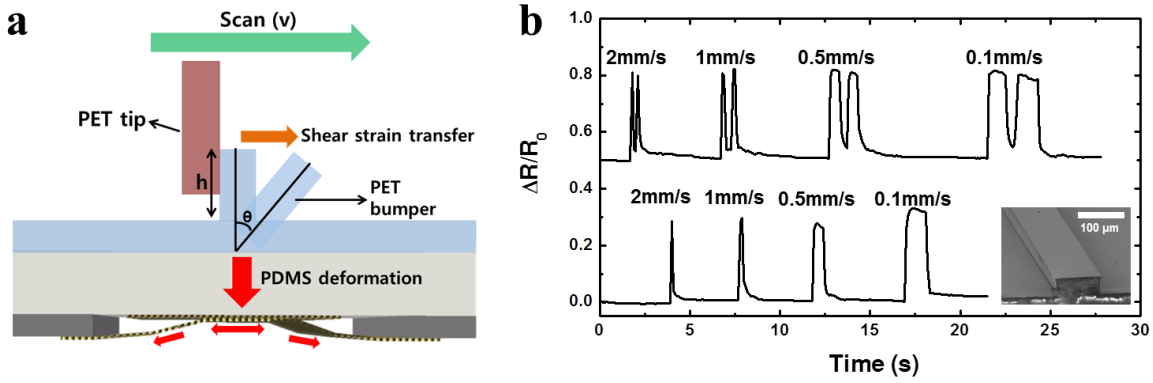

Fig. 4

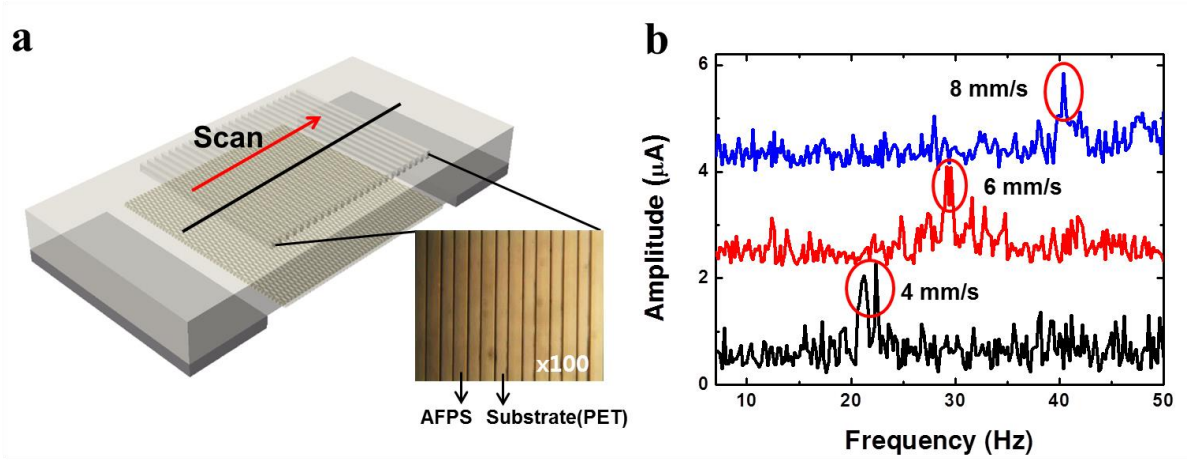

Fig. 5

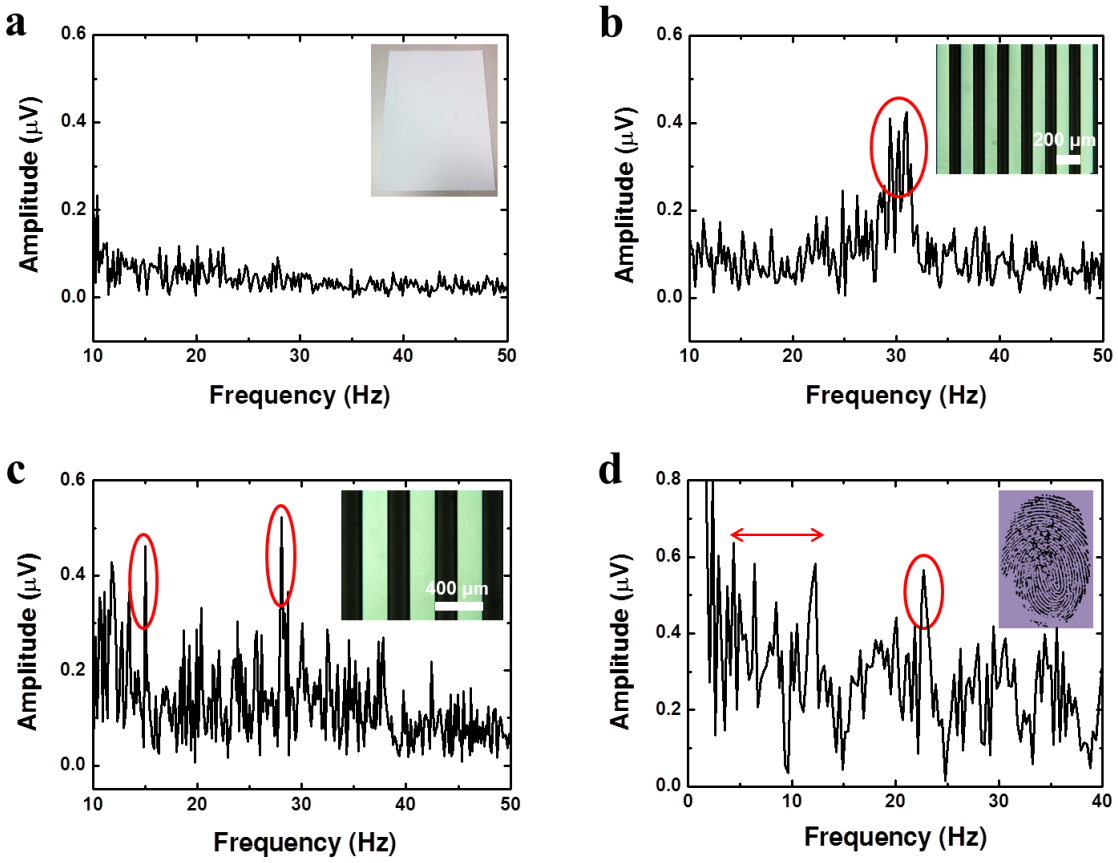

Fig. 6